Bilateral source acoustic interaction in a syrinx model of an oscine bird

Rodrigo Laje,[1,][*] Denisse Sciamarella,[2] Juan Zanella,[1] and Gabriel B. Mindlin[1]

[1]*Departamento de Física, FCEN, Universidad de Buenos Aires, Pabellón I, Ciudad Universitaria—C1428EGA, Buenos Aires, Argentina*
[2]*LIMSI-CNRS, Bôite Postale 133, F-91403 Orsay Cedex, France*

The bilateral simultaneous generation of sound in some oscine songbirds leads to complex sounds that cannot be described in terms of a superposition of the isolated sources alone. In this work, we study the appearance of complex solutions in a model for the acoustic interaction between the two sound sources in birdsong. The origin of these complex oscillations can be traced to the nonlinear mode-mode interaction arising when both sources are active. As an example, we analyze a remarkable sound produced by an oscine songbird and show that the proposed dynamical scenario is compatible with the observed behavior.

I. INTRODUCTION

The parallels between speech acquisition in humans and song learning in songbirds are striking [1,2]. Songbirds, like humans, depend critically on hearing a tutor during a sensory period where they form memories of the sounds they will later imitate, and also on hearing themselves during a sensorimotor period where they correct the vocal output through auditory feedback.

The capability of vocal imitation is not widespread, however. Apart from humans, only two distant groups of mammals are vocal learners: cetaceans, and some bats. In contrast, almost half the bird species known to exist (4000 out of 9000) share this capability: oscines, parrots, and hummingbirds [1]. The similarities and several experimental advantages [3] make these birds a very good animal model to study the brain mechanisms involved in the learning of a complex behavior. However, the avian vocal organ (the *syrinx*) stands between the neural instructions and the emitted sound. The syrinx is a nonlinear device which shows highly nontrivial solutions on its own—small variations in the control parameters such as air sac pressure can lead to a complex acoustic sequence [4]. Therefore, a knowledge of the syringeal dynamics is needed in order to understand how a neural instruction is translated into sound [5].

The mechanism of sound production in oscine songbirds is very similar to that used by humans to generate voiced sounds [6]. As it is forced through the syrinx, airflow from the air sacs induces the oscillation of small tissue masses called *labia*, which form a valve. This oscillation in turn modulates the airflow that is injected into the vocal tract as an acoustic disturbance. Perhaps one of the most important differences between the human larynx and the oscine syrinx is that the latter is a bilateral structure: there are two sound sources instead of only one, each containing a pair of labia. The two sound valves are capable of vibrating independently, and to some extent are also independently controlled [7]. Some birds use only one valve for singing, but some use both valves either alternatively or simultaneously [8]. Among the birds with simultaneous production, there are

some where the valves oscillate quite independently of each other ("two-voice" phenomenon), but in others the sound sources are coupled, giving rise to a complex sound that is more than the superposition of both sides alone.

Nonlinear interaction between the two sound sources was indeed demonstrated [9] in the call of the black-capped chickadee (*Parus atricapillus*). The equally spaced frequencies appearing in the call's spectrum were not always an integer multiple of their difference. Further, lesions to either side of the syrinx showed that these frequencies were sums and differences of integer multiples of the fundamental frequencies of the isolated sides (*heterodyne* frequencies). A linear summation of the signals from the isolated sides did not give rise to the spectrum of a normal call, suggesting that the heterodyne frequencies may result from a nonlinear interaction between the two syringeal sources. The physical mechanism responsible for such interaction, however, was speculative. Structural as well as acoustic interactions were considered [9,10].

On the other hand, nonlinear phenomena in the human voice have already been addressed by extensive modeling approaches. These nonlinear effects are usually related to voice disorders (like laryngeal paralysis) and even normal voices under certain conditions (like vocal fry and creaky voice). See, for instance, Ref. [11] for asymmetric vocal fold oscillations and Ref. [12] for biphonation.

Based on previous theoretical efforts [13–15], a model was recently proposed [16] to study the acoustic interaction between the avian source and tract, and between the two sources, with the isolated source considered as a two-dimensional (2D) dynamical system. In that work, the issue of a single source with delayed feedback due to acoustic coupling to the vocal tract was addressed. In this work we focus instead on the complementary case of the two sound sources simultaneously active, without feedback from the vocal tract. It was shown [4] that the isolated syrinx can display complex behavior by itself, like period-doubling bifurcations, mode locking, and nonperiodic dynamics. Accordingly, the isolated syrinx was modeled as a nonlinear system with several degrees of freedom (e.g., a two-mass model of the syrinx [4], or a membrane model [17]). Thus, in this work the choice of a simple (2D) model for the isolated sound source is dynamical in nature: any observed complex

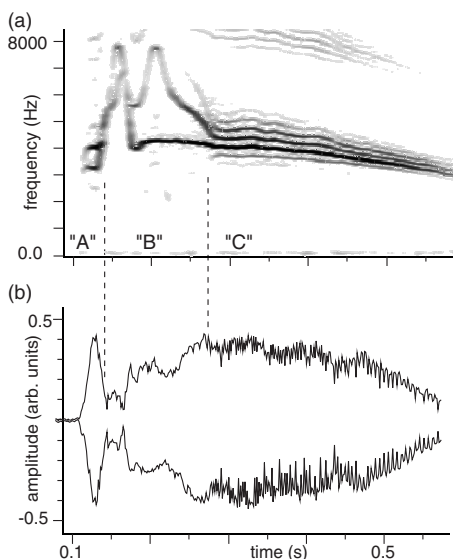---

*Corresponding author. rodrigo@df.uba.ar

FIG. 1. A syllable from the song of the magpie tanager (*Cissopis leveriana*) [18], an oscine songbird (bilateral syrinx with two sound sources). (a) Sonogram. In the interval labeled B, the two sound sources act independently. Something different apparently happens in intervals A and C, however, when the fundamental frequencies are close to each other and sidebands appear as parallel, additional strokes. The two sound sources seem to interact in some way, since the detailed time evolution of their fundamental frequencies now closely resemble each other. (b) Sound envelope. The occurrence of subharmonic frequencies and sidebands coincides with intervals of large sound amplitude and close fundamental frequencies (A and C). At the end of interval C the amplitude is small, but the frequencies are even closer. On the other hand, at the beginning of interval B the frequencies are very close but the amplitude is very small. Different renditions of the same sound by the bird share the same features described here.

behavior must arise only from the interaction between the two sound sources.

In Fig. 1 we show a remarkable sound by the magpie tanager (*Cissopis leveriana*) [18], a South American oscine songbird. Notice the two qualitatively different regimes. In segment B, the clearly different temporal and spectral evolution of the two dark strokes is a signature of the two sound sources being uncoupled and acting independently. However, in segments A and especially C the detailed time evolutions of the two dark strokes closely resemble each other although they are not harmonically related. In addition, several parallel strokes appear both above and below the original ones at frequency values that are not integer multiples of the frequencies of any of the original strokes, but at heterodyne frequencies (sums and differences of integer multiples of the fundamental frequencies). These heterodyne frequencies appear when the fundamental frequencies are very close and the sound amplitude is high. It is tempting to put forward several questions: What is the dynamical origin of the sidebands and subharmonic frequencies? Is acoustic coupling between the two sides of the syrinx a plausible physical origin for the interaction? Is the interaction turned on (or at least increased) when the fundamental frequencies of the sides are close enough?

In this work we study the acoustic interaction between the two sound sources as a plausible physical origin of subharmonic frequencies and sidebands in birdsong like those shown in Fig. 1. We show here that complex solutions due to nonlinear mode-mode interaction appear in a specific region of the parameter space of our model [16]. The system approaches that region along paths in parameter space that have a direct interpretation in terms of realistic motor gestures. In Sec. II the model for the acoustically coupled sound sources is presented, and the region worth exploring is suggested by the result of a normal form computation. In Sec. III the region is explored numerically, and solutions are shown with complex features resembling the ones presented by a paradigmatic sound in the song of a songbird. The dynamical origin of the spectrum's sidebands and its relationship with the concept of a nonlinear interaction as a multiplication of signals is explained in Sec. IV. Finally, Sec. V contains our conclusions.

II. MODEL FOR SOURCE-SOURCE ACOUSTIC INTERACTION

In a recent work [16], we proposed a model for the acoustic interaction in birdsong vocalizations and studied the particular case of acoustic interaction between source and tract, focusing on the mechanism that leads to a net energy transfer from airflow to labial motion. In this work, instead, we consider the original model ([16], "extended flapping model") and use it for the complementary case of the two sound sources active without feedback from the tract. In this case our model reads

$$\dot{x}_1 = y_1,$$

$$\dot{y}_1 = -k_1 x_1 - B y_1 - C x_1^2 y_1 + p_{g1}, \qquad (1)$$

$$\dot{x}_2 = y_2,$$

$$\dot{y}_2 = -k_2 x_2 - B y_2 - C x_2^2 y_2 + p_{g2}, \qquad (2)$$

$$p_{g1} = p_s - \left(\frac{x_0 + x_1 - \tau y_1}{x_0 + x_1 + \tau y_1} \right)(p_s - p_i), \qquad (3)$$

$$p_{g2} = p_s - \left(\frac{x_0 + x_2 - \tau y_2}{x_0 + x_2 + \tau y_2} \right)(p_s - p_i), \qquad (4)$$

$$p_i = \alpha_1(x_1 - \tau y_1) + \beta_1 y_1 + \alpha_2(x_2 - \tau y_2) + \beta_2 y_2, \qquad (5)$$

where subscripts 1 and 2 stand for the left and right sides of the syrinx, respectively. Here $x_{1,2}$ are the departures from the prephonatory positions of the labia midpoints, $k_{1,2}$ are the linear restitution coefficients, B and C are the linear and nonlinear dissipation coefficients, p_s is the air sac pressure, p_i is the pressure at the vocal tract input, x_0 is the prephonatory position of the labium (rectangular profile), τ is a phenomenological parameter that describes the speed of the labial surface wave, and $\alpha_{1,2}$ and $\beta_{1,2}$ are the acoustic coupling coefficients (which depend on the frequency but in this work

are assumed to be constant for simplicity) [16].

The forces p_{g1} and p_{g2} that account for the energy transfer from airflow to labial motion in order to sustain the oscillation are due to the interlabial pressure being created between the lateral and medial labia on each valve. They depend on the geometry of the valve profile, and on both the air sac pressure p_s and the pressure at the vocal tract input p_i. The latter depends on the variables from both sources and thus couples their dynamics.

A preliminary study of the solutions for a related system was presented in our previous work [16]. Here we attempt a further level of analysis in order to understand the dynamical origin of this model's rich behavior.

A. Approximations

In order to unveil the path worth exploring in parameter space, we first perform a third-order approximation to the geometric flapping quotient in Eqs. (3) and (4):

$$\frac{x_0 + x - \tau y}{x_0 + x + \tau y} \sim 1 - \frac{2\tau}{x_0}y + \frac{2\tau}{x_0^2}xy + \frac{2\tau^2}{x_0^2}y^2$$
$$- \frac{2\tau}{x_0^3}x^2y - \frac{4\tau^2}{x_0^3}xy^2 - \frac{2\tau^3}{x_0^3}y^3. \quad (6)$$

Within this approximation, the model [Eqs. (1)–(5)] can be rearranged in the more suitable form

$$\dot{x}_1 = y_1,$$

$$\dot{y}_1 = -\kappa_1 x_1 + \Pi y_1 - \Lambda x_1^2 y_1 + \gamma x_2 + \delta y_2$$
$$+ (\text{quadratic terms } x_1 y_1, y_1^2, x_2 y_1, y_1 y_2)$$
$$+ (\text{cubic terms } x_1 y_1^2, x_1 x_2 y_1, x_1 y_1 y_2, x_2 y_1^2, y_1^2 y_2, y_1^3),$$
$$(7)$$

$$\dot{x}_2 = y_2,$$

$$\dot{y}_2 = -\kappa_2 x_2 + \Pi y_2 - \Lambda x_2^2 y_2 + \gamma x_1 + \delta y_1$$
$$+ (\text{quadratic terms } x_2 y_2, y_2^2, x_1 y_2, y_2 y_1)$$
$$+ (\text{cubic terms } x_2 y_2^2, x_2 x_1 y_2, x_2 y_2 y_1, x_1 y_2^2, y_2^2 y_1, y_2^3),$$
$$(8)$$

where

$$\kappa_{1,2} = k_{1,2} - \alpha, \quad (9)$$

$$\Pi = 2\tau p_s/x_0 - B + \delta, \quad (10)$$

$$\Lambda = C - 2\tau(x_0\gamma + p_s)/x_0^3, \quad (11)$$

$$\gamma = \alpha, \quad (12)$$

$$\delta = \beta - \tau\alpha. \quad (13)$$

For simplicity, we choose the acoustic coupling parameters α and β to be symmetric. The only asymmetry in this model is then given by $k_1 \neq k_2$.

TABLE I. Parameter values.

Original parameters	Units
$8.2 \times 10^8 \leq k_1 \leq 1.8 \times 10^9$	(s^{-2})
$k_2 = 8 \times 10^8$	(s^{-2})
$0 \leq p_s \leq 2 \times 10^7$	(cm s^{-2})
$B = 1000$	(s^{-1})
$C = 5 \times 10^8$	(s^{-1} cm^{-2})
$\tau = 1 \times 10^{-5}$	(s)
$x_0 = 0.04$	(cm)
$\alpha = 3 \times 10^6$	(s^{-2})
$\beta = 700$	(s^{-1})

Derived parameters	Units
$8.17 \times 10^8 \leq \kappa_1 \leq 1.797 \times 10^9$	(s^{-2})
$\kappa_2 = 7.97 \times 10^8$	(s^{-2})
$-330 \leq \Pi \leq 4670$	(s^{-1})
$\Lambda = 4.97 \times 10^8$	(s^{-1} cm^{-2})
$\gamma = 3 \times 10^6$	(s^{-2})
$\delta = 670$	(s^{-1})

Note that the core of Eqs. (7) and (8) is the standard form of two generalized van der Pol relaxation oscillators. The oscillators are linearly coupled to each other through the terms $\gamma x_{2,1} + \delta y_{2,1}$. Regarding the coupling coefficients γ and δ, we additionally assume throughout the text the following *weak coupling approximation* (see the Appendix):

$$\frac{\gamma\delta}{\Delta\kappa} \ll \kappa_2^{1/2}, \quad \frac{\gamma^2}{\Delta\kappa} \ll \kappa_2, \quad \frac{\delta^2}{\Delta\kappa} \ll 1, \quad (14)$$

where $\Delta\kappa = \kappa_1 - \kappa_2 = k_1 - k_2$. Parameter values are listed in Table I. As we shall see, this standard set of values is sufficient for the system to have a rich behavior.

B. Normal form

Computation of the normal form for Eqs. (7) and (8) in the weak coupling approximation leads us to the following system for the mode amplitudes (see the Appendix):

$$\dot{r}_1 = \mu_1 r_1 + r_1^3 + b r_1 r_2^2, \quad (15)$$

$$\dot{r}_2 = \mu_2 r_2 + c r_2 r_1^2 + d r_2^3, \quad (16)$$

where μ_1 and μ_2 are the unfolding parameters. Guckenheimer and Holmes [19] showed that 12 different unfoldings for this system can be classified according to the signs of b, c, d, and $d - bc$. Within the weak coupling approximation, d and $d - bc$ are always positive, and thus according to the table on p. 399 of Ref. [19] only four cases are possible for our system (see the Appendix):
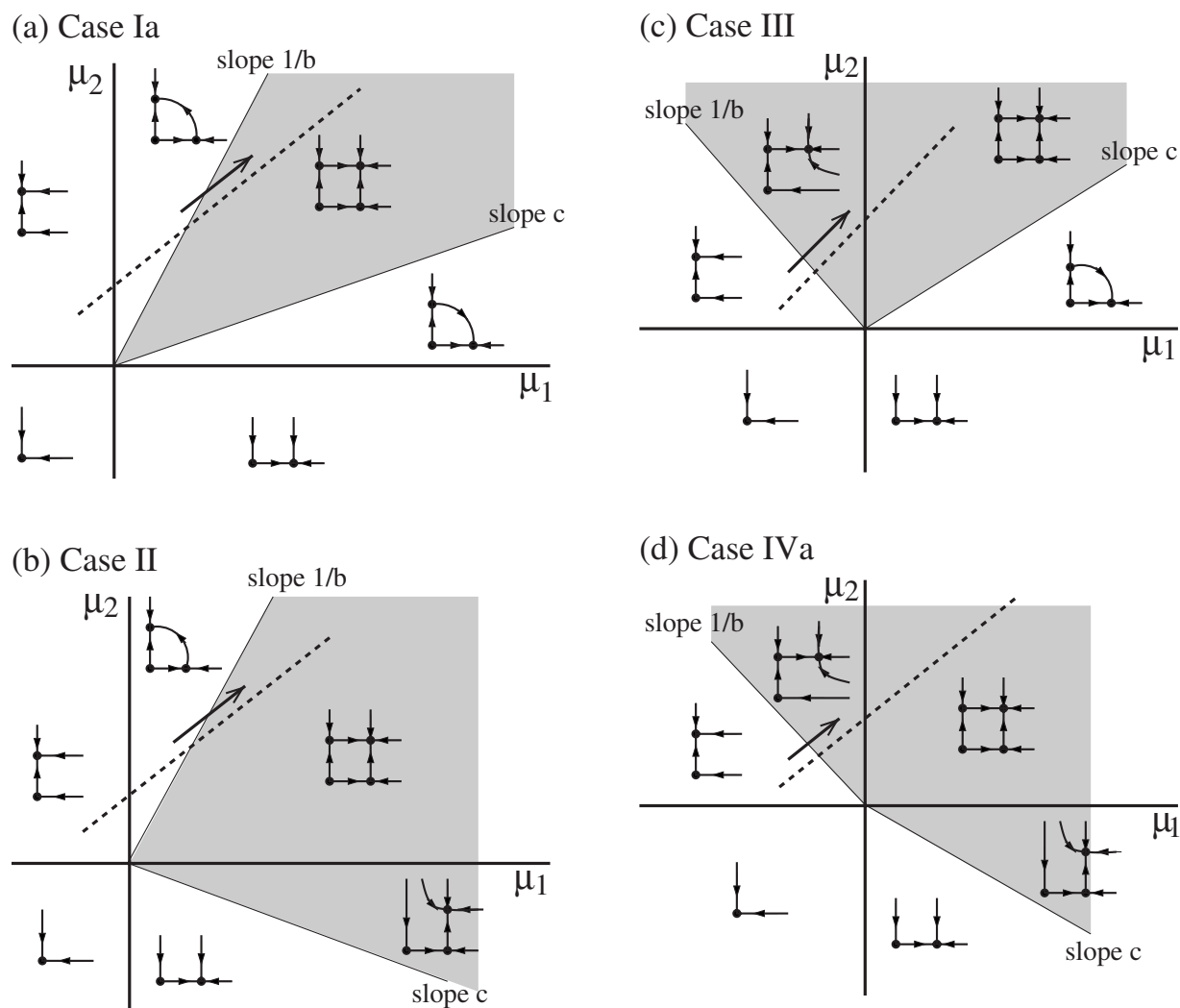
FIG. 2. Unfoldings for the system of Eqs. (15) and (16). (a) Case Ia. (b) Case II. (c) Case III. (d) Case IVa. Every unfolding has a nontrivial stable fixed point in the shaded regions. The dashed line [Eq. (17), with slope ~ 1 and perturbative offset from the origin] is the direction of increasing air sac pressure p_s. On increasing air sac pressure p_s, the system enters into the region of the nontrivial fixed point always very quickly, because its boundaries are always either very steep or very flat (slopes $|1/b| > 40$ and $|c| < 0.1$, respectively, for the parameter values listed in Table I).

	Case Ia	Case II	Case III	Case IVa
b	$+$	$+$	$-$	$-$
c	$+$	$-$	$+$	$-$

The unfoldings for these cases are displayed in Fig. 2. Notice that they all have a nontrivial stable fixed point in the first quadrant of the $(\mu_1; \mu_2)$ space, meaning that both modes are turned on. That is the region we should inspect in order to find complex solutions. What is a realistic path in parameter space that would allow us to inspect that region?

Much of the variety in songbird vocalizations can be accounted for by the action of the two model vocal gestures p_s and $k_{1,2}$ in Eqs. (1)–(5) [13,14]. These vocal gestures have a well-established interpretation in terms of physiological data (air sac pressure and ventralis Syringealis muscle activity, respectively). In the bird, the air sac pressure is related to the sound amplitude, while the vS muscle activity has a strong

positive correlation with the fundamental frequency. Therefore, we choose to inspect the solutions arising when p_s is increased, for arbitrary values of $\Delta k = k_1 - k_2$ (within the weak coupling aproximation). The direction of increasing air sac pressure p_s for arbitrary Δk is mapped onto the line

$$\mu_2 = \left(1 + \frac{2\delta^2}{\Delta\kappa}\right)\mu_1 + \frac{2\gamma\delta}{\Delta\kappa} \qquad (17)$$

(see the Appendix), which is displayed as a dashed line in the unfoldings of Fig. 2. The line has a slope ~ 1 (slightly depending on the value of $\Delta\kappa$) and a little offset from the origin. This assures us that the system enters the region of existence of the nontrivial fixed point when p_s is large enough.

III. SIMULATIONS

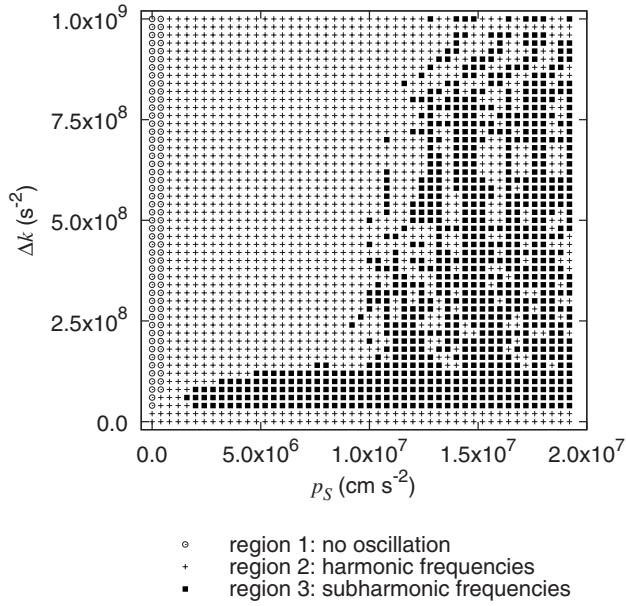In order to show that our model's behavior is consistent with the observed features of the sound displayed in Fig. 1,

○   region 1: no oscillation
+   region 2: harmonic frequencies
■   region 3: subharmonic frequencies

FIG. 3. Map of the spectral content of the model Eqs. (1)–(5) as a function of air sac pressure p_s and labial tension difference Δk $=k_1-k_2$ (k_2 is fixed at 8×10^8 s^{-2}). Region 1 (open circles): constant solutions, no oscillation takes place. Region 2 (crosses): periodic solutions with two independent frequencies F_1 and F_2 (the fundamental frequencies of the two modes, both active) and their corresponding harmonic overtones at integer multiples of them, nF_1 and mF_2 ("harmonic frequencies"), and no other frequencies. Region 3 (black squares): oscillatory solutions where heterodyne frequencies are found ("subharmonic frequencies"). Heterodyne frequencies are not integer multiples of the fundamental frequencies, but are sums and differences of integer multiples of them: nF_1 $+mF_2$, with $n,m \in \mathbb{Z}$. The Hopf-Hopf bifurcation takes place at the boundary between regions 1 and 2. Notice that the region 3 of subharmonic frequencies can be reached by either increasing air sac pressure p_s (and thus increasing sound amplitude) or decreasing the difference in labial tension between the sides Δk (and thus decreasing the difference between the fundamental frequencies). Parameter values other than p_s and k_1 are listed in Table I. The weak coupling approximation is not valid for the first few rows at the bottom ($\Delta k \sim 0.0$).

in this section we show numerical simulations along the line in parameter space given by Eq. (17), that is, increasing air sac pressure p_s for an arbitrary difference in labial tension between the sides $\Delta k=k_1-k_2$ (within the weak coupling approximation).

In Fig. 3 we show a map of the spectral content of our model's solutions, as a function of p_s and Δk. We found three distinct regions. In the first region (small p_s values) the solutions are not oscillatory. In the second and third regions the solutions are always oscillatory, but differ in their spectral content. In the second region, the spectrum has two very pronounced peaks (the fundamental frequencies of the modes F_1 and F_2) and several less pronounced peaks at integer multiples of each fundamental frequency (harmonic overtones nF_1 and mF_2, with $n,m \in \mathbb{N}$). The spectrum in this case can be described as the linear superposition of two independent harmonic spectra. On the other hand, the third region is dis-
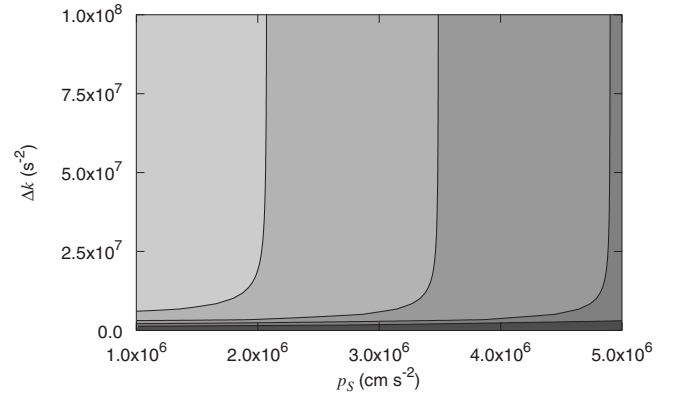
tinguished by its spectrum having, in addition, peaks at frequency values other than integer multiples of the two most pronounced peaks (for instance, at the heterodyne frequency values nF_1+mF_2, with $n,m \in \mathbb{Z}$). The shape of the boundary between regions 2 and 3 is a key feature of this system: the region of subharmonic frequencies can be approached by either increasing air sac pressure p_s (resulting in an increased sound amplitude) or decreasing labial tension difference Δk (resulting in closer fundamental frequencies), in qualitative agreement with the behavior observed in the syllable of Fig. 1.

The shape found in Fig. 3 can be understood in terms of the unfolding parameters μ_1 and μ_2. The length of the radius vector μ,

$$\mu = \sqrt{\mu_1^2 + \mu_2^2}, \qquad (18)$$

represents the distance from the Hopf-Hopf bifurcation (the origin in the unfoldings of Fig. 2) to a given point in parameter space. The larger the value of μ, the larger the distance from the bifurcation point. Complex solutions should be expected to be more likely the farther we go from the bifurcation point. In Fig. 4 we plot μ as a function of our control parameters p_s and Δk. Notice that μ increases (darker shading) either as p_s is increased or as Δk is decreased, meaning that the system moves farther away from the bifurcation point. There is a qualitative agreement between the shape of these contours and that of the boundary between regions 2 and 3 in Fig. 3.

Finally, we illustrate the behavior of our model with two simulations (Fig. 5), plotted as spectrograms of the acoustic pressure p_i. Two vocal maneuvers are simulated that make the system move from region 2 to region 3: an increase in the air sac pressure p_s, and a decrease in the labial tension difference Δk. The two simulations show a change in spectral content (appearance of subharmonic frequencies) as the control parameter is abruptly changed around 0.07 s.

FIG. 4. Contour plot of the radius vector μ in the unfolding parameter space, Eq. (18), as a function of air sac pressure p_s and labial tension difference Δk. Larger values of μ are represented by darker shading. μ is increased by either increasing p_s or decreasing Δk, moving the system farther from the bifurcation point. The shapes of these contours are in qualitative agreement with the shape of the boundary between regions 2 and 3 shown in Fig. 3.
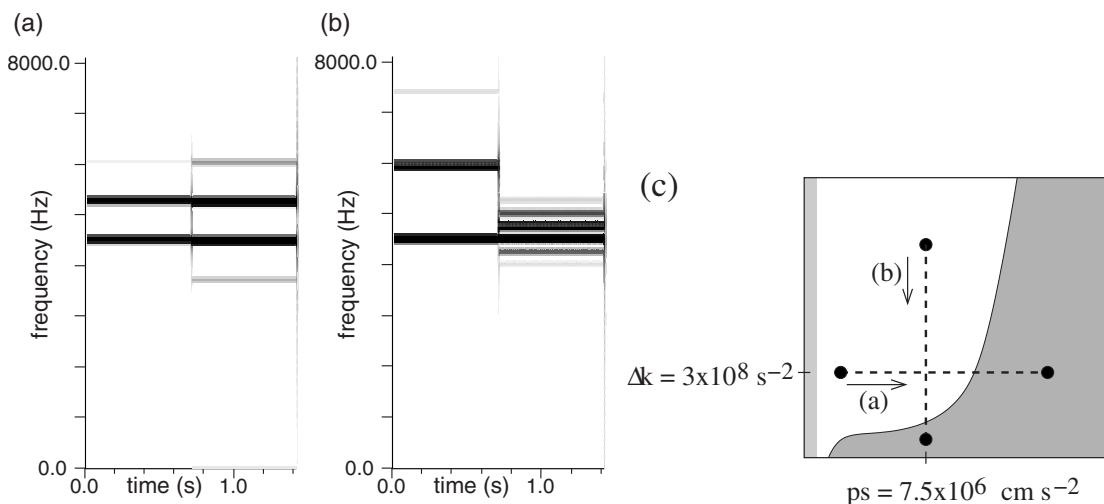
FIG. 5. Simulation of two different vocal maneuvers that move the system into region 3. In both cases the spectrogram of the resulting acoustic pressure p_i is plotted. (a) Air sac pressure p_s changes abruptly around 0.07 s, from 3×10^6 to 1.5×10^7 cm s^{-2}, and sidebands appear. Labial tensions are held constant at $k_1 = 1.1 \times 10^9$ s^{-2} and $k_2 = 8 \times 10^8$ s^{-2} ($\Delta k = 3 \times 10^8$ s^{-2}). (b) Labial tension k_1 changes abruptly around 0.07 s, from 1.4×10^9 to 9×10^8 s^{-2}, and sidebands appear. Parameters $k_2 = 8 \times 10^8$ s^{-2} and $p_s = 7.5 \times 10^6$ cm s^{-2} are held constant. (c) The two vocal maneuvers plotted as paths in parameter space of Fig. 3. Both cases show harmonic spectral content before the change in the control parameter (every frequency is an integer multiple of one of the two lowest frequencies). After the change, frequencies appear that are not integer multiples of the fundamental frequencies before. Transients not shown.

IV. DYNAMICAL ORIGIN OF SIDEBANDS IN THE SPECTRUM

The appearance of either heterodyne frequencies or sidebands (new frequency components close to an original fundamental frequency and not related harmonically to it) in a signal's spectrum is usually associated to the concept of *nonlinear interaction* between two harmonic oscillations [10]. The simplest model usually invoked to account for the nonlinear interaction of two oscillators is a nonspecific amplitude modulation of any of them, which leads to the multiplication of the two oscillations [10]. In mathematical terms, consider the (sinusoidal) amplitude modulation of a sinusoidal oscillation

$$
\begin{aligned}
f(t) &= A(t)\cos(\omega_1 t) \\
&= [1 + A_0 \cos(\omega_2 t)]\cos(\omega_1 t) \\
&= \cos(\omega_1 t) + A_0 \cos(\omega_2 t)\cos(\omega_1 t) \\
&= \cos(\omega_1 t) + \tfrac{1}{2}A_0 \cos(\omega_1 + \omega_2)t + \tfrac{1}{2}A_0 \cos(\omega_1 - \omega_2)t,
\end{aligned}
\tag{19}
$$

where we have used the trigonometric identity $\cos\alpha\cos\beta = \tfrac{1}{2}\cos(\alpha+\beta) + \tfrac{1}{2}\cos(\alpha-\beta)$. Equation (19) says that an oscillation at a frequency ω_1 which is modulated in amplitude at a frequency ω_2 (usually considered much smaller) yields a spectrum with the original frequency ω_1, plus two sidebands at $\omega_1 + \omega_2$ (slightly above ω_1) and $\omega_1 - \omega_2$ (slightly below ω_1). This simple and generic model, however, does not put forward any explanation about the way in which the two signals could actually become multiplied.

So amplitude modulation is a possible phenomenon leading to the multiplication of two signals, which is in turn a nonlinear operation and translates into sidebands in the spec-trum. But what is the dynamical origin of the multiplication? What is its relationship with the actual interaction?

In order to explicitly see the dynamical origin of the multiplication, consider two symmetrically coupled nonlinear oscillators

$$
\dot{x}_1 = y_1,
$$

$$
\dot{y}_1 = -\kappa_1 x_1 + \Pi_1 y_1 + f(x_1, y_1) + g(x_1, y_1, x_2, y_2), \tag{20}
$$

$$
\dot{x}_2 = y_2,
$$

$$
\dot{y}_2 = -\kappa_2 x_2 + \Pi_2 y_2 + f(x_2, y_2) + g(x_2, y_2, x_1, y_1), \tag{21}
$$

where $f(x, y)$ is nonlinear but the cross terms $g(x_1, y_1, x_2, y_2)$ can be either linear or nonlinear. In our model, for instance, the functions are $f(x, y) = -\Lambda x^2 y + O(2) + O(3)$ and $g(x_1, y_1, x_2, y_2) = \gamma x_1 + \delta y_1 + O(2) + O(3)$.

The following linear transformation to complex variables:

$$
(z_1, \bar{z}_1, z_2, \bar{z}_2) = C^{-1}(x_1, y_1, x_2, y_2), \tag{22}
$$

where C is the 4×4 matrix of the eigenvectors of the linear part of Eqs. (20) and (21) (the overbar denotes complex conjugation), leads us to the following diagonal system for the two modes of oscillation:

$$
\dot{z}_1 = (\mu_1 + i\omega_1)z_1 + a_1|z_1|^2 z_1 + c_1 z_1|z_2|^2 + G_1(z_1, z_2), \tag{23}
$$

$$
\dot{z}_2 = (\mu_2 + i\omega_2)z_2 + a_2|z_2|^2 z_2 + c_2 z_2|z_1|^2 + G_2(z_2, z_1). \tag{24}
$$

In amplitude-phase notation, the variables of the two modes of oscillation are
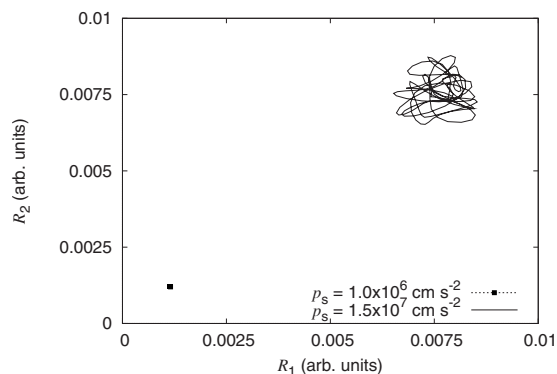
FIG. 6. Numerical integration of our model's Eqs. (7) and (8). R_1 and R_2 are the amplitudes of the two interacting modes defined by Eq. (25). A simulation with parameter values near the Hopf-Hopf bifurcation shows that both modes are turned on with constant amplitudes (the dot near the bottom left corner, $p_s = 1 \times 10^6$ cm s^{-2}). However, when the system is set far from the bifurcation ($p_s = 1.5 \times 10^7$ cm s^{-2}), the amplitudes of the modes R_1 and R_2 are not constant, but oscillatory. The spectrogram corresponding to this simulation is shown in Fig. 5(a) (second half). $\Delta k = 3 \times 10^8$ s^{-2}.

$$z_1 = R_1 \exp(i\phi_1), \quad z_2 = R_2 \exp(i\phi_2). \quad (25)$$

Note that near the double Hopf bifurcation the terms $G_{1,2}$ are not important, and thus Eq. (23) does not depend on the phase ϕ_2 of the second mode, because $|z_2|^2 = R_2^2$. Conversely, Eq. (24) does not depend on ϕ_1 because $|z_1|^2 = R_1^2$. A stable solution may exist where both modes are turned on (with constant amplitudes),

$$R_1 = R_{10}, \quad R_2 = R_{20}, \quad (26)$$

and their phases do not mix frequencies,

$$\phi_1 = \omega_1 t, \quad \phi_2 = \omega_2 t. \quad (27)$$

In this case, the transformation back to the original variables [Eq. (22)] yields a linear superposition of the two mode frequencies:

$$x_1(t) \sim R_{10} \cos(\omega_1 t) + R_{20} \cos(\omega_2 t). \quad (28)$$

This is illustrated in Fig. 6 (the stationary solution in the space of R_1, R_2).

On the other hand, when the system is not near the Hopf-Hopf bifurcation, the terms represented by $G_{1,2}$ become important and could mix frequencies. Consider, for instance, $G_1 = \epsilon z_1 z_2$ and $G_2 = \epsilon z_2 z_1$ [with ϵ a small, perturbative parameter; in our model, this term would be related, for instance, to the term $x_2 y_1$ in Eq. (7) which mixes position and velocity from different sides of the syrinx]. This will contribute a small term with ϕ_2 in the equation for $\dot{z}_1$, and a small term with ϕ_1 in that for $\dot{z}_2$. The effect will be that the mode amplitudes will be no longer constant, but have a perturbative dependence on time:

$$R_1 = R_{10} + R_{11}(\epsilon)\cos(\omega_2 t), \quad (29)$$

$$R_2 = R_{20} + R_{21}(\epsilon)\cos(\omega_1 t). \quad (30)$$

Back to the original variables: now it is easy to see the way in which the multiplication arises:

$$\begin{aligned} x_1(t) &\sim R_1(t)\cos(\omega_1 t) + R_2(t)\cos(\omega_2 t) \\ &= [R_{10} + R_{11}(\epsilon)\cos(\omega_2 t)]\cos(\omega_1 t) \\ &\quad + [R_{20} + R_{21}(\epsilon)\cos(\omega_1 t)]\cos(\omega_2 t) \\ &= R_{10}\cos(\omega_1 t) + R_{20}\cos(\omega_2 t) \\ &\quad + A_0(\epsilon)\cos(\omega_1 + \omega_2)t + B_0(\epsilon)\cos(\omega_1 - \omega_2)t, \end{aligned}$$

$$(31)$$

that is, the superposition of the two mode frequencies, plus two new frequencies (sum and difference). Similarly, other terms within $G_{1,2}$ would introduce other heterodyne frequencies in the spectrum. As we go farther from the Hopf-Hopf bifurcation, each mode amplitude will add more frequency components (the nonstationary solution displayed in Fig. 6).

In summary, the dynamical origin of the multiplication is that the amplitudes of the interacting modes are no longer constant when the system is far from the Hopf-Hopf bifurcation, but have a dependence on time.

V. CONCLUSIONS

In this work we analyzed the solutions of a model developed to study the acoustic interaction between the two sound sources and between source and tract in oscine songbirds. We restricted the model to the idealized case of the two sound sources alone (without a vocal tract) and showed that the subharmonic frequencies appearing in the solution's spectrum can be traced to the nonlinear mode-mode interaction arising when both modes are active. The proposed dynamical scenario is compatible with the analysis of a remarkable two-voiced sound by an oscine songbird. We conclude that acoustic interaction between the two sides of the syrinx must be taken into account as a possible physical mechanism of interaction.

Since the acoustic coupling coefficients α and β both depend on acoustic parameters like sound speed and air density [16], a possible way to test the source-source acoustic interaction hypothesis (acoustic coupling as the physical origin of the interaction between the two sound sources) is to perform a Heliox experiment in which a singing bird like the one of Fig. 1 is recorded in a much less dense atmosphere. Heliox is a gas mixture in which nitrogen, comprising 80% of ordinary air, is replaced with the less dense helium. A significant change in the spectral content (disappearance or attenuation of subharmonic frequencies) should be observed if the interaction is of acoustic nature. Heliox experiments were proposed to study the acoustic coupling between source and vocal tract [16].

APPENDIX

We start with our approximated system [Eqs. (7) and (8)] and compute the third-order normal form for the Hopf-Hopf bifurcation, keeping terms up to second order in the coupling coefficients γ and δ.

The matrix of the linear part of our system is

$$M = \begin{pmatrix} 0 & 1 & 0 & 0 \\ -\kappa_1 & \Pi_1 & \gamma & \delta \\ 0 & 0 & 0 & 1 \\ \gamma & \delta & -\kappa_2 & \Pi_2 \end{pmatrix}, \qquad (A1)$$

where we let $\Pi_1 \neq \Pi_2$ in order to be able to tune the Hopf-Hopf bifurcation. The condition for the single Hopf bifurcation in the uncoupled oscillators ($\gamma = \delta = 0$) is simply $\Pi_1^h = \Pi_2^h = 0$. For weak coupling, the condition for the Hopf-Hopf bifurcation (zero real part for both eigenvalues) is

$$\Pi_{1,2}^{hh} = \pm \frac{2\gamma\delta}{\Delta\kappa}, \qquad (A2)$$

where we have defined $\Delta\kappa = \kappa_1 - \kappa_2$ (assuming $\kappa_1 > \kappa_2$ without loss of generality). Notice that $\Pi_{1,2}^{hh}$ should be perturbative quantities, which is assured by requiring that

$$\frac{\gamma\delta}{\Delta\kappa} \ll \kappa_2^{1/2}. \qquad (A3)$$

In addition, we require every second-order term to be small. This is the *weak coupling approximation*:

$$\frac{\gamma\delta}{\Delta\kappa} \ll \kappa_2^{1/2}, \quad \frac{\gamma^2}{\Delta\kappa} \ll \kappa_2, \quad \frac{\delta^2}{\Delta\kappa} \ll 1. \qquad (A4)$$

The four eigenvalues of M evaluated at the Hopf-Hopf bifurcation are $\lambda_1, \bar{\lambda}_1, \lambda_2, \bar{\lambda}_2$, where

$$\lambda_1 = i\left(\sqrt{\kappa_1} + \frac{\gamma^2 - \kappa_1\delta^2}{2\sqrt{\kappa_1}\Delta\kappa}\right), \qquad (A5)$$

$$\lambda_2 = i\left(\sqrt{\kappa_2} - \frac{\gamma^2 - \kappa_2\delta^2}{2\sqrt{\kappa_2}\Delta\kappa}\right) \qquad (A6)$$

(i stands for the imaginary unit, $i^2 = -1$, and the overbar denotes complex conjugation). Note that the frequencies of the normal modes are very similar to those of the isolated sides of the syrinx $\sqrt{\kappa_1}$ and $\sqrt{\kappa_2}$. The corresponding four eigenvectors of M at the Hopf-Hopf bifurcation are $v_1, \bar{v}_1, v_2, \bar{v}_2$, where

$$v_1 = \left(1, \lambda_1, -\frac{\gamma + i\sqrt{\kappa_1}\delta}{\Delta\kappa}, -\frac{i\sqrt{\kappa_1}\gamma - \kappa_1\delta}{\Delta\kappa}\right), \qquad (A7)$$

$$v_2 = \left(\frac{\gamma + i\sqrt{\kappa_2}\delta}{\Delta\kappa}, \frac{i\sqrt{\kappa_2}\gamma - \kappa_2\delta}{\Delta\kappa}, 1, \lambda_2\right). \qquad (A8)$$

(Note that the leading order in γ, δ for the eigenvectors is only linear, although for the eigenvalues it is quadratic.) With this we can diagonalize the system by building the matrix

of the eigenvectors C and performing the usual linear transformation to complex variables $\mathbf{z} = C^{-1}\mathbf{x}$, where $\mathbf{z} \equiv (z_1, \bar{z}_1, z_2, \bar{z}_2)$ and $\mathbf{x} \equiv (x_1, y_1, x_2, y_2)$.

After this, we compute the quadratic transformation $\mathbf{z} = \mathbf{w} + \mathbf{h}_2(\mathbf{w})$ to variables $\mathbf{w} \equiv (w_1, \bar{w}_1, w_2, \bar{w}_2)$ that cancels out the quadratic terms in the diagonalized system, and explicitly make the replacement to obtain the normal form

$$\dot{w}_1 = \lambda_1 w_1 + A_{11}w_1|w_1|^2 + A_{12}w_1|w_2|^2, \qquad (A9)$$

$$\dot{w}_2 = \lambda_2 w_2 + A_{21}w_2|w_1|^2 + A_{22}w_2|w_2|^2. \qquad (A10)$$

Next we change to polar variables $w_{1,2} = r_{1,2}\exp(i\phi_{1,2})$ and obtain the normal form in radial variables

$$\dot{r}_1 = a_{11}r_1^3 + a_{12}r_1r_2^2, \qquad (A11)$$

$$\dot{r}_2 = a_{21}r_2r_1^2 + a_{22}r_2^3, \qquad (A12)$$

where $a_{ij} = \text{Re}(A_{ij})$. The resulting coefficients a_{12} and a_{21} are both first-order quantities in (γ, δ) and can be either positive or negative, depending on the parameter values, while a_{11} and a_{22} are both definite negative and of order 1:

$$a_{11} \sim -1 + O(\gamma) + O(\delta), \qquad (A13)$$

$$a_{12} \sim O(\gamma), \qquad (A14)$$

$$a_{21} \sim O(\gamma), \qquad (A15)$$

$$a_{22} \sim -1 + O(\gamma) + O(\delta). \qquad (A16)$$

We finally rescale to put the system in the form proposed by Guckenheimer and Holmes [19], p. 397:

$$\dot{r}_1 = \mu_1 r_1 + r_1^3 + br_1r_2^2, \qquad (A17)$$

$$\dot{r}_2 = \mu_2 r_2 + cr_2r_1^2 + dr_2^3, \qquad (A18)$$

where

$$b = \frac{a_{12}}{|a_{22}|}\text{sgn}(a_{11}) \sim O(\gamma), \qquad (A19)$$

$$c = \frac{a_{21}}{|a_{11}|}\text{sgn}(a_{11}) \sim O(\gamma), \qquad (A20)$$

$$d = \text{sgn}(a_{11}a_{22}) = +1. \qquad (A21)$$

Note that we performed a time scale change $t \to \text{sgn}(a_{11})t$ that is reversing, since for our system $\text{sgn}(a_{11}) = -1$.

A classification for the unfoldings of Eqs. (A17) and (A18) is given in [19], which depends on the signs of the parameters d, b, c, and $d - bc$. Here $d = +1$ and $d - bc \sim +1 + O(\gamma^2)$ are both positive definite. On the other hand, b and c

can be either positive or negative. Therefore only four cases are possible within this approximation, namely,

	Case Ia	Case II	Case III	Case IVa
b	+	+	−	−
c	+	−	+	−

The relationship between the unfolding parameters μ_1 and μ_2 in Eqs. (A17) and (A18) and the model parameters can be obtained by taking the real part of the eigenvalues (which vanish at the Hopf-Hopf bifurcation). It is given by

$$\mu_1 = \frac{1}{2}\left(\Pi_1 + \frac{(\Pi_2 - \Pi_1)\gamma^2 + (\Pi_1\kappa_2 - \Pi_2\kappa_1)\delta^2 - 2\Delta\kappa\gamma\delta}{\Delta\kappa^2 + \Pi_1^2\kappa_2 + \Pi_2^2\kappa_1 - \Pi_1\Pi_2(\kappa_1 + \kappa_2)}\right),$$

(A22)

$$\mu_2 = \frac{1}{2}\left(\Pi_2 + \frac{(\Pi_1 - \Pi_2)\gamma^2 + (\Pi_2\kappa_1 - \Pi_1\kappa_2)\delta^2 + 2\Delta\kappa\gamma\delta}{\Delta\kappa^2 + \Pi_1^2\kappa_2 + \Pi_2^2\kappa_1 - \Pi_1\Pi_2(\kappa_1 + \kappa_2)}\right).$$

(A23)

From this we can map the path in parameter space examined in this work, that is, $\Pi_1 = \Pi_2 \equiv \Pi$, onto the appropriate path in the space of the unfolding parameters $(\mu_1; \mu_2)$. By evaluating μ_1 and μ_2 in $\Pi_1 = \Pi_2 \equiv \Pi$ and then solving for μ_2, it can be shown that the path corresponding to increasing air sac pressure, that is, increasing Π, is mapped onto

$$\mu_2 = \left(1 + \frac{2\delta^2}{\Delta\kappa}\right)\mu_1 + \frac{2\gamma\delta}{\Delta\kappa},$$

(A24)

which is a line with slope ~ 1 and very little offset from the origin.

[1] M. S. Brainard and A. J. Doupe, Nature (London) **417**, 351 (2002).

[2] A. J. Doupe and P. K. Kuhl, Annu. Rev. Neurosci. **22**, 567 (1999).

[3] E. A. Brenowitz, D. Margoliash, and K. W. Nordeen, J. Neurobiol. **33**, 495 (1997).

[4] M. S. Fee, B. Shraiman, B. Peseran, and P. P. Mitra, Nature (London) **395**, 67 (1998).

[5] G. B. Mindlin and R. Laje, *The Physics of Birdsong* (Springer-Verlag, Berlin, 2005).

[6] F. Goller and O. N. Larsen, J. Comp. Physiol. [A] **188**, 841 (2002).

[7] F. Goller and R. A. Suthers, Nature (London) **373**, 63 (1995).

[8] R. A. Suthers, Nature (London) **347**, 473 (1990).

[9] S. Nowicki and R. R. Capranica, Science **231**, 1297 (1986).

[10] S. Nowicki and R. R. Capranica, J. Neurosci. **6**, 3595 (1986).

[11] I. Steinecke and H. Herzel, J. Acoust. Soc. Am. **97**, 1874 (1995).

[12] P. Mergell and H. Herzel, Speech Commun. **22**, 141 (1997).

[13] T. Gardner, G. Cecchi, M. Magnasco, R. Laje, and G. B. Mindlin, Phys. Rev. Lett. **87**, 208101 (2001).

[14] R. Laje, T. J. Gardner, and G. B. Mindlin, Phys. Rev. E **65**, 051921 (2002).

[15] G. B. Mindlin, T. J. Gardner, F. Goller, and R. Suthers, Phys. Rev. E **68**, 041908 (2003).

[16] R. Laje and G. B. Mindlin, Phys. Rev. E **72**, 036218 (2005).

[17] N. H. Fletcher, J. Theor. Biol. **135**, 455 (1988).

[18] R. Straneck, *Canto de las Aves de Misiones I* (LOLA, Buenos Aires, 1990).

[19] J. Guckenheimer and P. Holmes, *Nonlinear Oscillations, Dynamical Systems, and Bifurcations of Vector Fields* (Springer-Verlag, New York, 1983).